

# **3.36 PROJECT FINAL REPORT**

## **5/14/14**

### **Mimicking Hardwoods Using Honeycombs Manufactured from Acrylonitrile Butadiene Styrene (ABS): A Comparison of Mechanical Properties**

Patrick Dixon  
Keri Mroszczyk

#### **ABSTRACT:**

Wood has been used as a material to build mechanical structures for thousands of years. As a natural composite of cellulose fibers embedded in a matrix of lignin, this organic, cellular solid resists both tension and compression. Its properties depend on the direction of loading of its cells – whether radially, tangentially, or axially – and such anisotropy is modeled well as a regular honeycomb structure. With the development of rapid prototyping technologies using materials that resist rot, it is advantageous to investigate the ability of a 3D printed honeycomb to model the mechanical properties of wood.

Open-cell, hexagonal honeycomb structures with densities spanning those of hardwoods were fabricated using acrylonitrile butadiene styrene. The mechanical properties of the honeycombs were compared to those reported for each of the woods to ultimately assess the quality of the mimicking. Specimens for each relative density were printed and compressed by loading along the out-of-plane axis (axial) as well as the in-plane axis (transverse).

While the printed honeycombs proved to be less stiff than the reported values for wood, the trends in the relative densities agree with the models. This study is novel, as it uses a 3D printer to mimic the wood structure and thus develops important insight into mimicking the natural material with a thermoplastic. Additionally, this work explores the use honeycomb models at high relative densities similar to wood.

# I. Introduction

## *1.1 Background*

### **1.1.1 Wood**

Wood is a ubiquitous construction material, utilized in different product forms for myriad purposes, from furniture and bridges, to musical instruments and baseball bats [1,2]. The wood structure is orthotropic and cellular, and the material has remarkably different properties depending whether it is loaded radially, tangentially, or axially. The greatest anisotropy of wood is evident in comparing the properties when loaded along (axially) or across the grain (tangentially). The anisotropy is comparable to that seen in open-cell honeycombs where a honeycomb's in-plane (axial) properties differ from those out-of-plane (transverse). Similarly, the majority of wood is made up of long cells, so while it may be considered a closed-cell honeycomb, the end caps contribute little to the structural properties of the wood [3].

More detail regarding the wood structure is necessary to understand its unique mechanical attributes. At the molecular level, wood is composed of semi-crystalline cellulose, amorphous hemicellulose and lignin [4,5]. The cell walls, which make up the solid portion of the wood, are multilayered and consist of cellulose micro-fibrils embedded in a lignin-hemicellulose matrix [5]. The composition of the solid cell wall of wood varies little among different species such that its physical properties are assumed to be constant [3,6]. Thus, the differences from species to species are principally governed by the cellular structure.

The taxonomic differences that divide wood into two categories, softwoods and hardwoods, are also reflected in their cellular structures [1,2,7,8]. Softwoods are more homogenous than hardwoods, and the vast majority of their structure (90-95% by

volume) consists of long, fiber-like cells called tracheids, which provide both support and nutrient and water conduction [2,3,7]. The majority of the remaining tissue is made up ray cells, most of which are radially oriented parenchyma cells [2,7]. This relatively homogenous structure is commonly considered to resemble that of a honeycomb [3,6]. Softwood material (at 12% moisture content) has a Young's modulus that ranges from about 7 to 14 GPa, a compressive strength that ranges from about 20 to 50 MPa, and a density that ranges from  $300 \text{ kg/m}^3$  to  $600 \text{ kg/m}^3$  [1].

The structure of hardwoods, however, is more heterogeneous [1-3,7,9]. Rays and tracheids constitute some of the tissue [2], though the long, thick-walled fiber cells, which constitute 37-70% of the wood by volume, provide most the mechanical support [3,7]. Wide, low-density cells, known as vessels provide fluid and nutrient conduction and are the third major element of hardwood tissue. They generally constitute at least 10% of the tissue of hardwoods [2,3,7]. This varied structure gives hardwoods a broader range of density and mechanical properties. Two tropical hardwoods provide bounds for the density range: low density balsa at  $120 \text{ kg/m}^3$  and lignum vitae at  $1200 \text{ kg/m}^3$  [2]. The density range of most North American hardwoods is from  $600 \text{ kg/m}^3$  to  $800 \text{ kg/m}^3$  [1]. Assuming a solid cell wall density of  $1500 \text{ kg/m}^3$  for wood [10,11], the majority of hardwoods fall well above the cellular solid range of relative densities, and would technically be labelled porous solids [3]. The wall thickness to edge length ratio of the fibers is greater than this range in most cases as well, since the vessels reduce the overall density. In addition, the honeycomb-like structure becomes more of an approximation due to the different cell types.

Despite the high density and complicated structure of hardwoods, their structure and properties are still effectively modeled using honeycombs [3,6]. The equations for modelling of wood with this method are summarized in **Table 1**.

**Table 1. Modeling Properties of Wood [3]**

<i>Transverse properties (In-plane)</i>	<i>Axial properties (Out-of-plane)</i>
$\frac{E_T^*}{E_S} \propto \left(\frac{\rho^*}{\rho_S}\right)^3$ (1)	$\frac{E_A^*}{E_S} \propto \left(\frac{\rho^*}{\rho_S}\right)$ (2)
$\frac{\sigma_T^*}{\sigma_{ys}} \propto \left(\frac{\rho^*}{\rho_S}\right)^2$ (3)	$\frac{\sigma_A^*}{\sigma_{ys}} \propto \left(\frac{\rho^*}{\rho_S}\right)$ (4)

Hardwoods' axial properties as a function of density are proportional to density, and the transverse properties show good correspondence with in-plane honeycomb density dependences. Modelling wood with this approach does not assume or attempt to identify constants of proportionality, unless solid cell wall properties are identified or assumed.

Due to wood's high performance (high strength and stiffness at low density), a great deal of work has been performed to emulate the wood structure with ceramics, through biotemplating [12]. Additionally to combine the sustainability and mechanical properties of wood with the processability of thermoplastics, wood-plastic composites are gaining ground in industry [13]. The work described in this report, provides an interesting combination of these ideas, trying to mimic the wood structure with plastics alone.

### **1.1.2 Acrylonitrile Butadiene Styrene (ABS)**

ABS is a common terpolymer that is sold in the largest volume of all engineering thermoplastics worldwide. This popular material is used for applications in automotive parts, refrigerator linings, medical equipment, and pipes and fittings[14]. In regards to its molecular composition, ABS consists of discrete, cross-linked polybutadiene (PB) rubber particles, which are grafted with poly(styrene-co-acrylonitrile) (SAN) and then embedded in a SAN matrix [14]. This microscale structure results in a macroscale thermoplastic that

is pliable at a given temperature and solidifies upon cooling, due to the intermolecular interactions of the crosslinks. It is commonly sold as pellets and then molded for the desired application.

The exact composition of the ABS is tunable given that the crosslink density and latex particle size can be altered during production, and thus its range of physical and mechanical properties reflect the nature of its chemical composition. Its properties depend on the two phases: a hard, transparent and brittle thermoplastic (SAN), and an elastomeric phase containing the crosslinked PB. The commercially available injection-grade polymer, used for 3D printing and extrusion applications have rubber loadings of 15-20% and S/AN ratios in the SAN of 75/25 with completely grafted particles [14]. Typically, ABS has densities between 1.05 and 1.07g/cm<sup>3</sup>. Its physical properties are between those of rubber and glass, however, mechanically, it resembles glass more than it does rubber [14]. The elastic modulus for the two-phase system follows the simple rule of mixtures. Commercially available compositions have an average elastic modulus of 2.30 GPa and a yield strength of 43.2 MPa. The average Poisson's ratio for ABS is 0.4 [14].

The development of rapid prototyping (RP) technologies has allowed easy fabrication of structures based on a computer-aided design, specifically with ABS. An ABS filament is fed through a heating element, which heats it to a semi-molten state. Using a nozzle, the 3D printer then deposits the filament onto the partially constructed part. Since the material is deposited at semi-molten state, the newly added filaments fuse with adjacent material that has already been laid down for the structure [15].

The structure's mechanical properties are affected by the directionality in which the filaments are deposited (**Fig. 1**). The directionality is determined by the orientation of

the structure in which as little supporting or fill material is required to maintain the integrity of the structural design during printing, while the filaments fuse together. The build direction causes anisotropic behavior of 3D printed parts, and subsequently, the strength of the material is dependent on the orientation of the filaments, to a certain extent [15].

In a previous study using three rapid prototyping processes, a specimen's compressive strength was shown to depend on the direction of filament deposition (**Fig. 1**). In comparing the dependence of compressive strength on directionality of ABS from a similar rapid prototyping process to 3D printing, known as fused deposition modelling (FDM), the FDM specimen's compressive strength was 41.26MPa, when filaments were parallel to the loading, which was 11.6% higher than the perpendicular loading case. [15]. Additionally, it is important to note that the resolution of the printer constrains the target density of the printed samples [16].

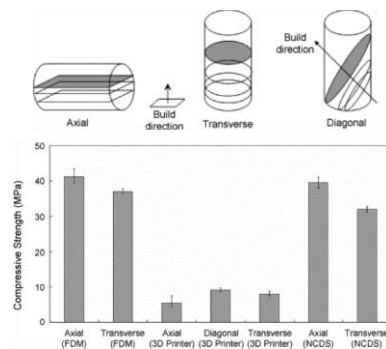


**Figure 1.** Representation of the deposition of filaments and the corresponding variation in compressive strengths [15]

Building regular, hexagonal honeycombs, requires consideration of the direction of filament deposition as well as the build-direction requiring the least amount of fill to form proper cell voids in the structure. Even with this consideration, rapid prototyping allows facile construction of cellular structures such as honeycombs, which have

widespread use in thermal isolation, lightweight sandwich panels, and energy absorption. Further, these cellular solids are ubiquitous in nature and provide plants with mechanically sound structures with little weight [3].

With the development of 3D printing, the relative density of a honeycomb structure can be adjusted by simply adjusting the input file to the 3D printing software. In this manner, synthetic honeycombs mimicking biological structures can be finely tuned and even improved with hierarchical organizations [16]. Honeycombs printed with ABS have been shown to have a relatively broad range of elastic properties and the range of mechanical behavior can be adjusted by tailoring the two dimension ratios and the structural organization of hierarchical honeycombs [16].

Despite the widespread study of 3D printing with ABS in recent years, there has been limited work to use this thermoplastic to model wood. Prior studies have investigated combining sawdust and ABS to create composites for adhesion mechanisms and improving interfacial strengths [17]. These experiments used an injection-molding machine to fabricate specimens. As the content of sawdust in the mixture was increased, there was a reduction in the composite strength, since the ABS tough-matrix was disrupted by rigid wood sawdust particles, impairing stress transfer under load. The results suggested that as the content of sawdust content increased, the moduli increased with progressive decreases in the strength of the composites [17]. While the ABS-sawdust composite does not outperform either of the materials alone, this study demonstrates the ability to improve adhesion and compatibility between polar cellulose fibers and hydrophobic polymers. With the success in creating ABS-sawdust composites, the challenge remains to understand the potential of ABS alone to provide the mechanical

integrity that wood affords. To improve upon the application of ABS to natural structures, this present study aims to assess the ability of honeycombs made of ABS to model the properties of wood.

### **1.2 Objective**

The goal of the project was to fabricate 3 different open-cell, hexagonal honeycomb structures with densities representative of the hardwood density range using ABS, apply and assess honeycomb models to the high relative density ABS honeycombs, and compare the mechanical properties to those reported for hardwoods to ultimately assess the quality of our mimicking. In support of this objective, honeycombs of three different densities mimicking hardwoods were loaded along the in-plane and out-of-plane axis to determine the compressive strength and Young's modulus to compare the honeycombs to known values of wood from the literature.

### **1.3 Significance**

ABS is commonly used in investigations relating honeycomb geometries and mechanics, due to its high processability [18]. The widespread use of wood-plastic composites in construction indicates a growing need for a synthetic alternative to wood without sacrificing the material's natural mechanical properties and low weight [13,19]. A synthetic alternative would also overcome the challenge of rot and degradation with time and weather, increasing the life and safety of the structure. Specifically, ABS is resistant to chemical degradation from acidic or alkaline solutions [14]. Efforts to design a synthetic wood structure improves the understanding of the effects of the organization of fibers in the different wood models.

## II. Methods

### 2.1 Processing

The three density honeycomb templates were drawn in SolidWorks<sup>®</sup>. The honeycomb structures consisted of regular hexagons, of varying thickness to edge length ratio ( $t/l$ ), which were chosen to mimic the density of woods. This ratio, and thus the relative density, was adjusted by changing the inner edge length of the hexagons and wall thickness. The inner edge lengths of the design from low to high density were as follows: 3 mm, 3 mm, and 2 mm. The corresponding wall thicknesses were 0.79 mm, 2.55 mm, and 3.55 mm respectively. To calculate the design ( $t/l$ ), the edge length,  $l$  was estimated as the sum of the inner edge length and wall thicknesses. The resulting design ratios then were 0.208, 0.459, and 0.636, for low, medium to high density respectively. The honeycomb structures were printed as blocks of 2 in (width) x 2 in (thickness) x 2 in (length) with a Dimension<sup>®</sup> bst 1200es 3D printer, using *ABSPlus*, a type of ABS created for 3D printing. To produce specimens appropriately sized for the load cell, the blocks were cut in half perpendicular to the out-of-plane axis for transverse specimens, and in fourths, parallel to the out-of-plane axis, for axial specimens. These provided in-plane specimens of roughly 50.8 mm (width) x 25.4 mm (thickness) x 50.8 mm (length) and out-of-plane specimens of 25.4 mm (width) x 25.4 mm (thickness) x 50.8 mm (length). See appendix for images of the specimens (**Figs. A1, A2**).

### 2.2 Mechanical Testing

Specimens were compressed along their lengths for loading in both directions using an Instron testing machine. A crosshead speed of 0.05 mm/s was used, and the load was measured with a 45 kN load cell. Attaching an extensometer to a honeycomb was not feasible for these tests and thus a measurement of displacement normalized by the body

length was used for an approximate strain measurement. The experimental properties (transverse Young's moduli and compressive strength) were compared with those of wood, and modeled based on the calculated properties and the observed deformation mode.

### III. Results

The prepared honeycombs were relatively defect-free (see **Figs. A1 & A2** for images of structures), and the densities of all honeycombs of the same type (low, medium, and high density) were similar. Average values of densities were 326, 538, and 716 kg/m<sup>3</sup>. Taking a solid density of  $\rho_s = 1040$  kg/m<sup>3</sup>, from the *ABSPlus* specification sheet [20], the relative densities were calculated as 0.31, 0.52, and 0.69. The actual densities of honeycombs mimic those of high-density balsa, Oregon ash, and red oak, respectively. The largest standard deviation in density among the three types was that of the high density honeycombs, at  $\pm 7$  kg/m<sup>3</sup>, giving a coefficient of variation of about 1%. The densities of the tested specimens (both in- and out-of-plane specimens) is shown in **Fig. 1** with respect to the wall thickness edge length ratio,  $(t/l)$  from the Solidworks files. The solid line plotted is a geometry-density relationship of equation 5, with  $\rho_s = 1040$  kg/m<sup>3</sup>.

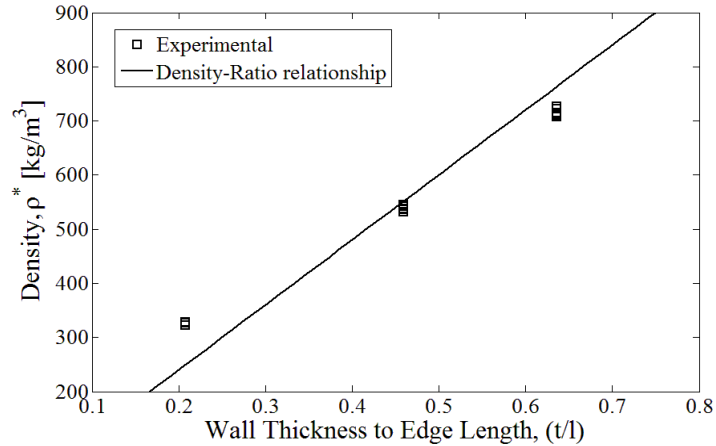


**Figure 1.** Density plotted against design ( $t/l$ )

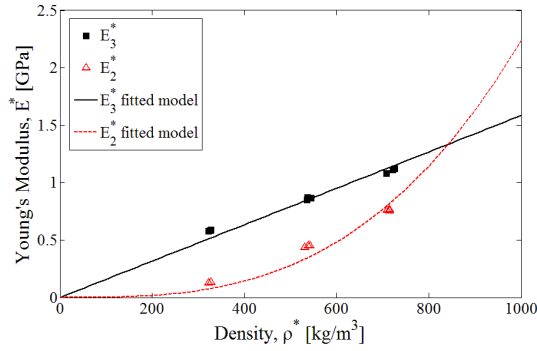
Four wall thicknesses were measured on one specimen of each density and averaged. An additional specimen of the low density was used to take six measurements, as the design wall thickness and the printed thickness differed. The average wall thicknesses in mm, in order of increasing density were:  $1.175 \pm 0.063$ ,  $2.520 \pm 0.022$ , and  $3.418 \pm 0.057$ . All agree with the design  $t$  (see **Methods**), except the low density honeycomb.

In-plane specimens of all densities did not show clear plateaus. Densification was not observed, but specimens were not tested to strains where densification would be observed, as the load dropped sharply and the maximum load was near the limit of the load cell. For the in-plane specimens, failure seemed to occur by plastic yielding of the cell walls, followed by cell wall fracture (**Fig. A3** gives images of failed in-plane honeycombs). Color changes in the cell walls, and deviation from non-linear behavior before failure suggested plastic yielding of the cell walls in bending. Failure in specimens of all densities was highly apparent at the vertices. The in-plane specimens did not show a clear plateau. Since, the cell walls fractured, a serrated plateau would be expected. However, the load generally dropped continuously and steeply up to strains of 12%, and

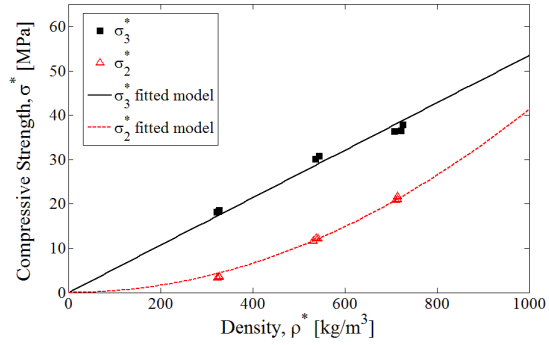
any serrations that were observed were over large increments of strain (e.g. **Fig. A5**). For this reason the peak in compressive stress was taken as the strength.

The out-of-plane specimens did exhibit stress plateaus, but again, specimens were not strained high enough for densification to be observed because of the limit of the load cell. The failure mode observed for the out-of-plane specimens was uniaxial plastic yielding, as no visible signs of failure were evident, during the beginning of the plateau, in most cases. The final structures did show deformation that resembled plastic buckling (**Fig. A4**). However these instabilities only formed after significant strain following the stress plateau. In the case of the high density honeycombs, an ABS casing was noticeably printed at the boundary of the structure. During out-of-plane loading, this casing delaminated from the structure, and may have resulted in lower strength values (**Fig. A6** show this structure and its delamination). Since many of the plateaus were slightly negative, the minimum between the intercept of the tangents to the elastic and plateau regions of the stress-strain curve and the maximum stress on the stress-strain curve was defined as the out-of-plane strength.

**Fig. 2** displays the out-of-plane and in-plane Young's moduli (**2(a)**) and compressive strengths (**2(b)**) of the ABS honeycombs. Models described in the following section are plotted as well. The properties in both directions increase with density, though their specific dependences on density are not clear from the plot, and are addressed in the following in section 3.1.



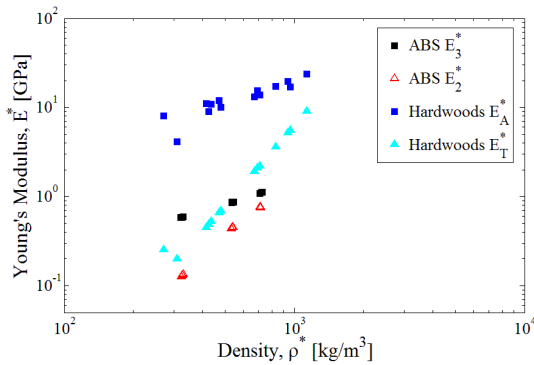
2(a)



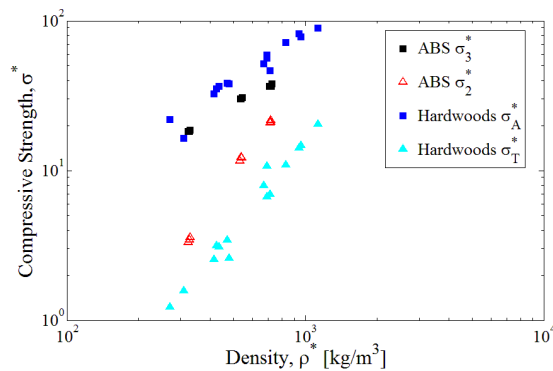
2(b)

**Figure 2.** Young's modulus and compressive strength of ABS honeycombs (3 = out-of-plane, 2 = in plane)

The same experimental data are shown in **Fig. 3**, but now on logarithmic axes. The same properties of several hardwoods over the wood density range, taken from the materials selection database CES Selector<sup>®</sup> [21], are also plotted. **Fig. 3(a)** shows the Young's moduli, and **Fig. 3(b)** plots the compressive strengths. The different density dependences are more clearly seen from the figure.



3(a)



3(b)

**Figure 3.** Young's modulus and compressive strength of ABS honeycombs and hardwoods (3 = out-of-plane, 2 = in plane, a = axial, t = transverse) [21]

### 3.1 Modelling

The approach used to model the mechanical properties was that of “fitted models.” Experimental data was fitted with functions of forms that match the theory for

the particular property, direction, and failure mode as described by the results (see **Table 2**). The curves were fitted with the MATLAB Curve Fitting Toolbox, using polynomial functions.

**Table 2.** Properties of Regular Hexagonal Honeycombs [3]

<i>In-plane properties</i>	<i>Out-of-plane properties</i>
$\frac{\rho^*}{\rho_s} = \frac{2}{\sqrt{3}} \left(\frac{t}{l}\right) = 1.15 \left(\frac{t}{l}\right)$ (5)	
$\frac{E_2^*}{E_s} = \frac{3}{2} \left(\frac{\rho^*}{\rho_s}\right)^3$ (6)	$\frac{E_3^*}{E_s} = \frac{\rho^*}{\rho_s}$ (7)
Yielding (in bending) $\frac{(\sigma_{pl}^*)_2}{\sigma_{ys}} = \frac{1}{2} \left(\frac{\rho^*}{\rho_s}\right)^2$ (8)	Plastic buckling $\frac{(\sigma_{pl}^*)_3}{\sigma_{ys}} \approx 4.4 \left(\frac{\rho^*}{\rho_s}\right)^{5/3}$ for $v_s = 0.3$ (10)
Rupture (in bending) $\frac{(\sigma_{cr}^*)_2}{\sigma_{fs}} = \frac{1}{3} \left(\frac{\rho^*}{\rho_s}\right)^2$ (9)	Uniaxial yielding $\frac{(\sigma_{pl}^*)_3}{\sigma_{ys}} = \left(\frac{\rho^*}{\rho_s}\right)$ (11)

For example, the in-plane Young's modulus,  $E_2^*$ , was fit with respect to density, using a third order polynomial, with only the cubed term (eqn 6). The resulting fit was:

$$E_2^* = (2.2 * 10^{-9})(\rho^*)^3 = \frac{3}{2} E_s \left(\frac{\rho^*}{\rho_s}\right)^3 \quad r^2 = 0.92 \quad (12)$$

By taking the constants of proportionality of regular hexagons, as in **Table 2**, and a solid cell wall density of  $\rho_s = 1040 \text{ kg/m}^3$ , a solid cell wall modulus of  $E_s = 1.65 \text{ GPa}$  was estimated. Similarly for the out-of-plane Young's modulus,  $E_3^*$  the fit (now linear and proportional, eqn 7) was

$$E_3^* = (1.59 * 10^{-3})(\rho^*) = E_s \left(\frac{\rho^*}{\rho_s}\right) \quad r^2 = 0.96 \quad (13)$$

This estimated a solid cell wall modulus as  $E_s = 1.65 \text{ GPa}$ .

The fitting of the compressive strength gave in-plane (eqn 8) and out-of-plane (eqn 11) fits respectively as

$$\sigma_2^* = (4.14 * 10^{-5})(\rho^*)^2 = \frac{1}{2} \sigma_{ys} \left(\frac{\rho^*}{\rho_s}\right)^2 \quad r^2 = 0.99 \quad (14)$$

$$\sigma_3^* = (5.35 * 10^{-2})(\rho^*) = \sigma_{ys} \left(\frac{\rho^*}{\rho_s}\right) \quad r^2 = 0.97 \quad (15)$$

This fit estimated an in-plane solid cell wall yield strength of  $\sigma_{ys} = 89.6$  MPa, and an out-of-plane solid cell wall yield strength of  $\sigma_{ys} = 55.6$  MPa. If cell wall fracture was the dominate failure mechanisms in-plane, with the constant of proportionality of regular hexagons, the solid cell wall modulus of rupture would be  $\sigma_{fs} = 134.3$  MPa (eqn 9).

These models (eqn. 12-15) are plotted on **Fig. 2**. The extrapolated properties with those from literature are shown below in **Table 3**.

**Table 3.** Solid ABS Properties

	<b>In-Plane</b>	<b>Out-of-Plane</b>	<b>Literature (measured) [14]</b>
<b>E<sub>s</sub> [GPa]</b>	1.65	1.65	2.3
<b>σ<sub>s</sub> [MPa]</b>	89.6	55.7	43.2

Given the fact that there are essentially only three data points (three close clusters of three), linear fits of the in-plane data show good correlation ( $r^2 \sim 0.99$ ). Making the fits proportional as well as linear, severely reduces the quality of the correlation ( $r^2 \sim 0.77$ ). In an attempt to verify the models, the data were fit to power law functions with respect to density, so that the exponents could be compared to those dictated by the theory. The exponents of the power law fit are 2.07 and 0.81 for the in and out of plane Young's moduli respectively, and 2.16 and 0.85 for the in and out of plane compressive strengths. All exponents, when rounded, agree with the theory, except in the case of the in-plane Young's moduli. For details regarding these equations see the Appendix.

## IV. Discussion

All of the honeycombs had a high relative density; the lowest density that was measured was on the boundary of transition between cellular and porous solids, and the others by strict definition would be porous solids. However, the aim of this study was to mimic wood over its vast density range, and there are hardwoods with comparable relative densities. Considering a solid wood cell wall density as  $1500 \text{ kg/m}^3$ , examples of wood corresponding to the relative densities measured in this study are bigleaf maple (several softwoods have this relative density), shagbark hickory, and bloodwood [1], [2].

The actual densities versus those expected by the simple geometric relationship show discrepancies (**Fig. 1**). The largest disagreement occurred for the low-density honeycomb. Initially this was surprising as the relationship (eqn. 5) is valid for low densities. The printed wall thickness of 1.175 mm, however, was not the same as the design  $t$ , 0.79 mm. The Dimension<sup>®</sup> bst 1200es 3D printer either does not provide resolution less than a millimeter, or the printer software did not properly read the files. Since the measured  $t$  of the other honeycombs agreed with the design, it is likely that printing of the low density honeycomb was resolution-limited. If the measured  $t$  was used the estimated  $(t/l)$  becomes 0.281. This ratio predicts a density of  $336 \text{ kg/m}^3$ , which agrees well with the measured values. The middle density honeycomb agrees well with the relationship, but the relationship over predicts the density of the densest honeycombs; this difference is not large or unexpected, as the relationship is meant to model low densities.

These calculations of relative densities suggest that regular hexagon honeycomb constants of proportionality in mechanical models are a reasonable approximation. In general, the mechanical models match the data quite well (**Fig. 2**). As previously mentioned, several simple mathematical functions would fit the data well, which questions whether the models are representative of the reality of deformation. The models merit further discussion.

The fitted model for the in-plane Young's moduli had the lowest correlation coefficient. The in-plane moduli for the low and middle densities were under predicted, while the high density was slightly over predicted. Additionally, it was the only property, for which the exponent of the power-law fit, 2.07, did not round to the exponent dictated by the theory: 3. For these reasons, the model for the in-plane moduli seems the most problematic. A possible explanation is that at relatively high densities ( $\rho^*/\rho_s > 0.3$ ), initial elastic deformation may have enough axial compression character causing both bending and axial deformation, and giving an exponent of two (an average of the exponents corresponding to bending (three) and axial deformation (one)). However, plasticity seemed to be governed by bending, as the power law exponent rounds to two.

The out-of-plane moduli model describes the data quite well. This is not unexpected, as the rule of mixtures forms the basis for the equation, and when the honeycombs are axially loaded the initial deformation is uniaxial. The power-law exponent, 0.81, is less than 1, which is dictated by the theory, but does not greatly disagree with the model, as was the case for the out-of-plane modulus. Both the in-plane and out-of-plane models use and predict the same fully dense Young's modulus,  $E_s = 1.65$  GPa.

Both models of compressive strengths have high correlation coefficients and graphical agreement with the data. Exponents from the power-law fits – 2.16 and 0.85 for in plane and out of plane, respectively – agree with the theory. Thus, the strength models sufficiently represent the data.

The mode of failure, however, is still questionable. All of the honeycombs were too dense for the cell walls to have elastically buckled in either direction. For the in-plane loading, it is possible that the mode of failure was cell wall fracture. However, color change in the cell walls and nonlinear deviation on the stress-strain curve suggests that there was yielding prior to cell wall fracture. Additionally, this failure behavior has the same density dependence as yielding, so the fitted model would not change. The value of the estimated solid cell wall property changes to the solid cell wall modulus of rupture at 134.3 MPa (using regular hexagon constants, eqn 9). This value is quite high for ABS and most engineering plastics [21] and seems to be an indication that plastic yielding governed failure, although it is possible that the constant of proportionality for cell wall fracture of regular hexagons is incorrect at these high densities. The out-of-plane failure, which was observed as uniaxial yielding, is quite logical considering that at these relative densities the equation for plastic buckling predicts higher strength values than that of uniaxial yield (**eqn 10**).

The extrapolated Young's moduli of the solid cell wall are the same value. However, the value of 1.65 GPa falls below the range of Young's modulus of ABS (1.9 to 3 GPa) and it is lower than that given for ABSPlus, 2.32 GPa [20,21] (see **Table 3**). Two likely causes are: (1) the supplier of *ABSPlus* overstates its properties and (2) measuring the strain from the crosshead displacement lead to artificially lower values

from edge effects. While the second seems far more likely, it is surprising that the estimated values are the same. The extrapolated strength properties differ, and the in-plane solid cell wall strength, 89.6 MPa is significantly higher than the out-of-plane value 55.6 MPa and at the upper end of the range of compressive yield strengths [20,21]. The differing strength values may be due to the difference in the “grain” direction, as in both specimens the layers were printed in the out-of-plane direction.

These models are theoretically based, and the experimental results partially verified the theory. High density breakdowns in the models are not directly apparent. If the printed solid properties were found to be consistent with the extrapolated solid cell wall properties, a stronger conclusion could be stated.

Differences in the mechanical properties of wood and ABS honeycombs are clear (**Fig. 3**). The Young’s moduli of the ABS honeycombs are lower than that of wood, especially in the out-of-plane/axial case. This seems logical given the difference between the solid properties of ABS and those of the crystalline cellulose, which has an impressive Young’s modulus on the crystalline axis,  $\sim 140$  GPa, and is a major constituent of wood and highly oriented on the axial direction [6, 11]. The compressive strengths are more comparable, with the out-of-plane values lower than that of wood, and the in-plane values higher. This difference in material properties accounts for the difference between our mimicking ABS honeycombs and that of a honeycomb composed of lingo-cellulosic fibers. Further, the brittle nature of ABS gives the failure more fracture type character than that of wood.

There are other important considerations in comparing the ABS honeycombs to the natural structures. Firstly, ABS is hydrophobic allowing it to resist mechanical

changes due to environmental cues whereas the hydrophilic and hygroscopic nature of cellulose causes problems of dispersion and moisture absorption [19]. Interfacial forces between the two materials do not agree; the intramolecular hydrogen bonding system of cellulose provides the natural structure with variations in flexural rigidity compared to the homogenous, hydrophobic ABS. The roughness of the surfaces of wood allows irregularities to immediately be filled by water [19], which provides wood and cellulose with greater compliance compared to the more brittle cell walls of the ABS honeycomb.

#### **4.1 Limitations**

Similarly modeling the wood structure as a honeycomb has certain limitations. There are differences between the macroscopic structure of softwoods, ring-porous hardwoods, and diffuse-porous hardwoods that are not included in the regular honeycomb model. Further, sap channels, vessels, cell caps and knots in the biological specimen result in additional anisotropic considerations not included in the honeycomb models ABS [3]. In comparing the synthetic honeycomb to the natural structure, it is important to note that the ABS honeycomb was printed by first laying down an outline of the structure, which created a casing around the core material of the honeycomb and introduced heterogeneity in the material properties of the honeycomb. Upon examination of the deformed specimens, there was clear delamination of the casing from the core of the honeycomb. While ABS is advantageous since it resists rot, cellulose composites have many advantages compared to traditional inorganic ones: they come from a renewable and abundant resource, are less damaging to the environment, are recyclable and biodegradable and most importantly, they combine relatively low cost with favorable mechanical properties [19].

## V. Conclusion

The study of ABS honeycombs provides two important insights. Firstly, at high relative densities, honeycomb models developed for relative densities less than 0.3 seem appropriate for ABS; the relationship between density and  $(t/l)$  (eqn. 5) for low-density, regular hexagonal honeycombs relates the two parameters well at high relative densities. Further, mechanical data are described well by functions with density dependences based on theory. These conclusions provide support for the modelling of wood as a honeycomb over its full density range, despite its high relative densities. Secondly, obtaining a high stiffness with the low weight of wood using synthetic materials is difficult. Though, in this study, ABS was the only material tested, and no attempts were made to add high performance fiber reinforcement. It is hypothesized that while adding reinforcement would allow the possibility of reaching similar performance as wood, processing would become difficult and complex quickly, specifically with fiber alignment. Taken together, this study successfully outlined the success and the challenges associated with modeling wood structures with 3D printed honeycombs.

## VI. References

- [1] Forest Products Service, *Wood Handbook*. Madison, Wisconsin: Forest Products Laboratory USDA, 2010.
- [2] R. B. Hoadley, *Understanding Wood: A Craftsman's Guide to Wood Technology*. Newton, CT: The Tauton Press, Inc., 2000.
- [3] L. J. Gibson and M. F. Ashby, *Cellular Solids: Structure and Properties*, 2nd ed. Cambridge, UK: Cambridge University Press, 1997.
- [4] D. Fengel and C. Wegener, *Wood: Chemistry, Ultrastructure, Reactions*. Munich: Verlag, 2003.
- [5] S. Andersson, H. Wikberg, E. Pesonen, S. L. Maunu, and R. Serimaa, "Studies of crystallinity of Scots pine and Norway spruce cellulose," *Trees - Struct. Funct.*, vol. 18, no. 3, pp. 346–353, May 2004.
- [6] L. Mishnaevsky and H. Qing, "Micromechanical modelling of mechanical behaviour and strength of wood: State-of-the-art review," *Comput. Mater. Sci.*, vol. 44, no. 2, pp. 363–370, Dec. 2008.
- [7] J. M. Dinwoodie, *Timber: Its Nature and Behavior*, 2nd ed. London: E & FN Spon, 2000.
- [8] J. C. F. Walker, *Primary wood processing: principles and practice*, 2nd ed. Dordrecht: Springer, 2006.
- [9] W. Stelte and A. R. Sanadi, "Preparation and Characterization of Cellulose Nanofibers from Two Commercial Hardwood and Softwood Pulps," *Ind. Eng. Chem. Res.*, vol. 48, no. 24, pp. 11211–11219, Dec. 2009.
- [10] R. M. Kellogg and F. F. Wangaard, "Variation in the cell-wall density of wood," *Wood Fiber Sci.*, vol. 1, no. 3, pp. 180–204, 1969.
- [11] L. J. Gibson, "The hierarchical structure and mechanics of plant materials," *J. R. Soc. Interface*, vol. 9, no. 76, pp. 2749–2766, Nov. 2012.
- [12] M. Mizutani, H. Takase, N. Adachi, T. Ota, K. Daimon, and Y. Hikichi, "Porous ceramics prepared by mimicking silicified wood," *Sci. Technol. Adv. Mater.*, vol. 6, no. 1, pp. 76–83, Jan. 2005.
- [13] A. Wechsler and S. Hiziroglu, "Some of the properties of wood–plastic composites," *Build. Environ.*, vol. 42, no. 7, pp. 2637–2644, Jul. 2007.
- [14] M. Adams, D. Buckley, and R. Coburn, "Acrylonitrile-butadiene-styrene polymers." 1993.
- [15] C. S. Lee, S. G. Kim, H. J. Kim, and S. H. Ahn, "Measurement of anisotropic compressive strength of rapid prototyping parts," *J. Mater. Process. Technol.*, vol. 187–188, pp. 627–630, Jun. 2007.
- [16] A. Ajdari, B. H. Jahromi, J. Papadopoulos, H. Nayeb-Hashemi, and A. Vaziri, "Hierarchical honeycombs with tailorable properties," *Int. J. Solids Struct.*, vol. 49, no. 11–12, pp. 1413–1419, Jun. 2012.
- [17] L. Chotirat, K. Chaochanchaikul, and N. Sombatsompop, "On adhesion mechanisms and interfacial strength in acrylonitrile–butadiene–styrene/wood sawdust composites," *Int. J. Adhes. Adhes.*, vol. 27, no. 8, pp. 669–678, Dec. 2007.
- [18] Whelan, T., et al., *Injection molding of thermoplastic materials -1, Acrylonitrile Butadiene Styrene*, Springer US, 1990.
- [19] G. Cantero, A. Arbelaiz, F. Mugika, A. Valea, and I. Mondragon, "Mechanical Behavior of Wood/Polypropylene Composites: Effects of Fibre Treatments and Ageing Processes," *J. Reinf. Plast. Compos.*, vol. 22, no. 1, pp. 37–50, Jan. 2003.
- [20] Stratasys, "ABSPlus-P430," 2013 .
- [21] Granta Design, "CES Selector," 2014.

## Appendix

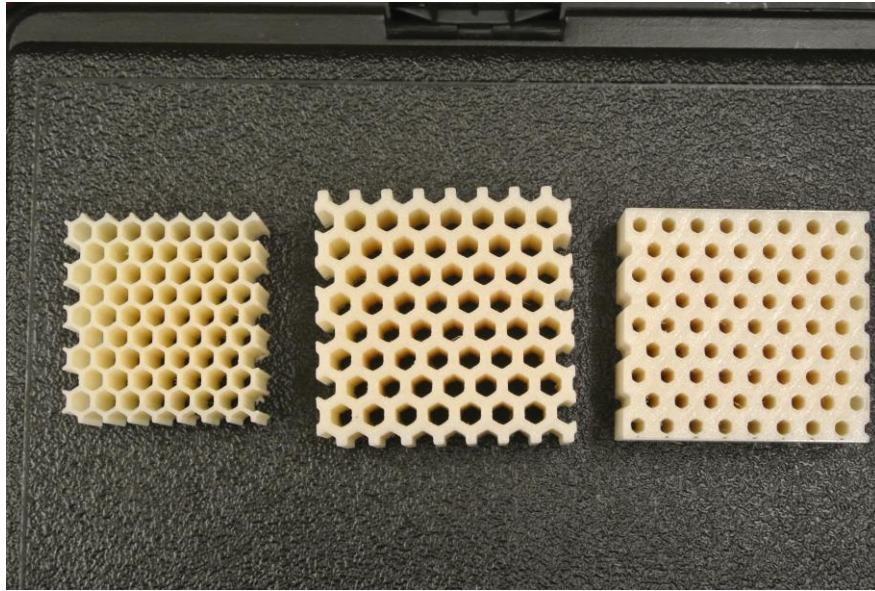


**Figure A1.** In-plane Specimens

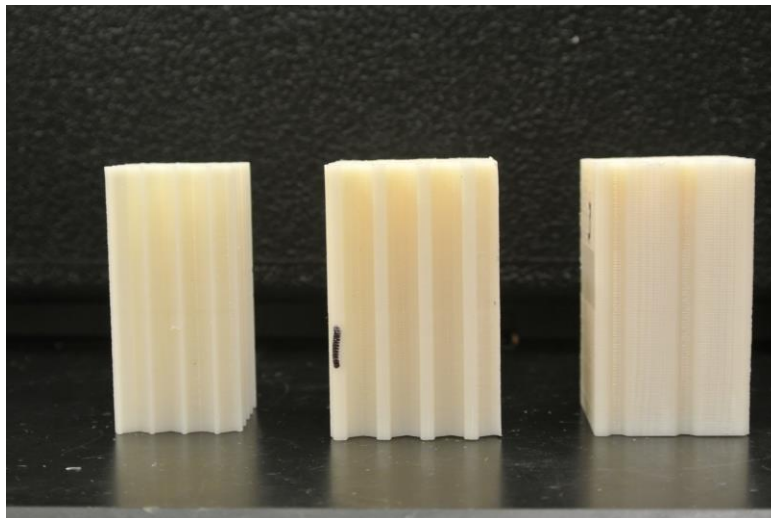


**Figure A2.** Out-of-plane Specimens

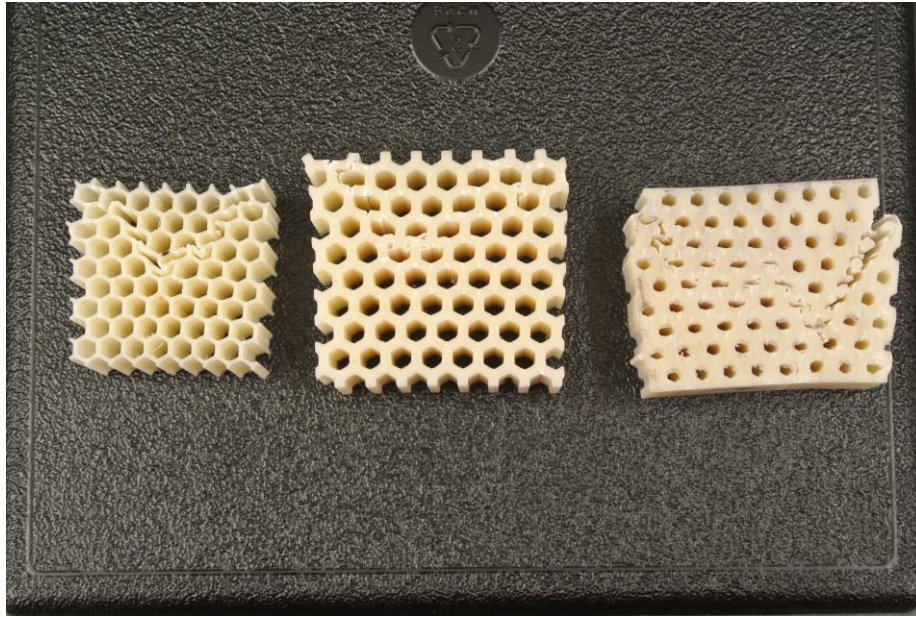


**Figure A3.** Tested in-plane specimens

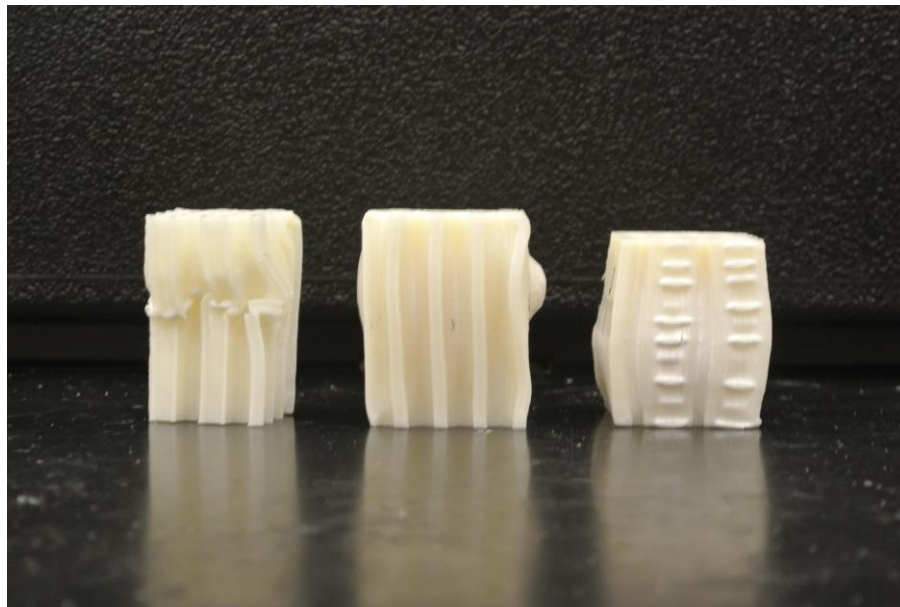


**Figure A4.** Tested out-of-plane specimens

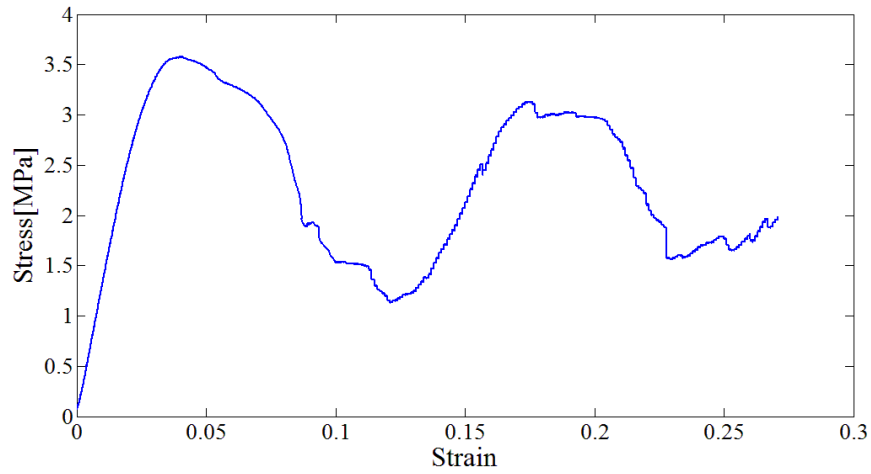


**Figure A5.** Sample stress strain curve, low density, in-plane

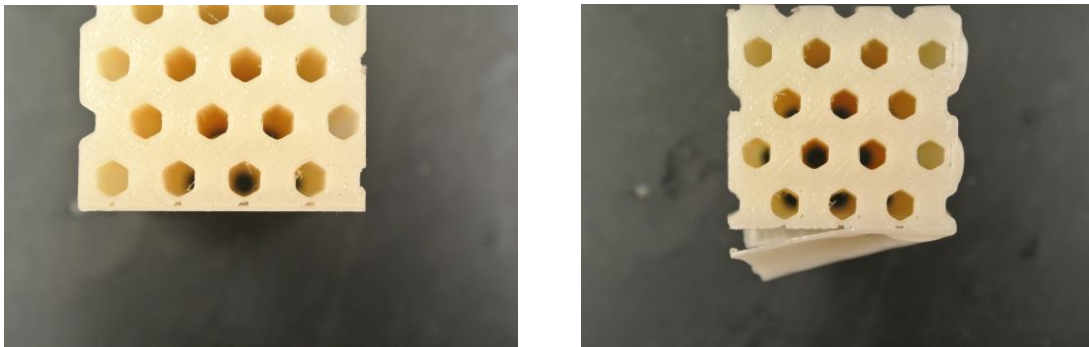


**Figure A6.** Casing on high density honeycombs

Power Law Fits

$$E_2^* = (9.6 * 10^{-7})(\rho^*)^{2.07} \quad r^2 = 0.99$$

$$E_3^* = (5.32 * 10^{-3})(\rho^*)^{0.81} \quad r^2 = 1$$

$$\sigma_2^* = (1.46 * 10^{-5})(\rho^*)^{2.16} \quad r^2 = 1$$

$$\sigma_3^* = (1.32 * 10^{-1})(\rho^*)^{0.85} \quad r^2 = 0.99$$

MIT OpenCourseWare  
<http://ocw.mit.edu>

3.054 / 3.36 Cellular Solids: Structure, Properties and Applications  
Spring 2015

For information about citing these materials or our Terms of Use, visit: <http://ocw.mit.edu/terms>.